

# Markov-chain approach to a process with long-time memory

Guglielmo Lacorata

Dipartimento di Fisica, Università di Roma “La Sapienza” Italy, and

Dipartimento di Fisica, Università de L’Aquila, Italy

Rubén A. Pasmante

Royal Dutch Meteorological Institute, Netherlands

Angelo Vulpiani

Dipartimento di Fisica, INFN and SMC,

Università di Roma “La Sapienza”, Italy

February 9, 2020

## **Abstract**

We show that long-term memory effects, present in the chaotic dispersion process generated by a meandering jet model, can be nonetheless taken into account by a first order Markov process, provided that the states of the phase space partition, chosen to describe the system, be appropriately defined.

## **1 Introduction**

Geophysical processes often exhibit an irregular behavior that is due to deterministic chaos and/or to the presence of many relevant degrees of freedom. Striking examples are climate dynamics (Fraedrich 1988, Nicolis et al. 1997) and transport processes in the atmosphere and in the oceans where many different characteristic temporal scales are involved (Samelson 1992, Yang 1996). After Lorenz's seminal work (Lorenz 1963), it is now well recognized that even deterministic systems with as few as three degrees of freedom can have complex temporal evolution similar to genuine stochastic processes (Ott 1993, Beck and Schlögl 1993). For example, the large-scale and long-time dispersion characteristics of drifters deterministically advected by a non-stochastic velocity field, giving rise to Lagrangian chaos, can, sometimes, be

well described by random walk models (Ottino 1989, Crisanti et al. 1991). On the other hand, a simple probabilistic description, e.g., one in terms of autoregressive models and Markov chains (Vautard et al. 1990, Nicolis et al. 1997), is often not able to catch the richness of most geophysical phenomena.

In a recent paper (Cencini et al. 1999), mixing and transport in a meandering jet were investigated and compared with a Markov chain. It was found that, due to the presence of very different characteristic time scales, this simple approach was not fully satisfactory. In fact, the ubiquitous presence of a hierarchy of time scales forces one to develop nonstandard techniques for data analysis and for their modeling.

The main aim of this Note is to show how a suitable Markov chain with a small number of states can reproduce in a proper way the main statistical features of systems similar to the one that is considered below. The basic point is an appropriate definition of the states of the system, such that long-time memory effects are straightforwardly taken into account in a Markov chain approximation of the dynamics. We expect this kind of analysis to be of interest in the more general context of systems with multiple time scales.

## 2 Transport in a meandering jet

The test case under consideration consists of a 2D meandering jet, formerly introduced as a model for studying Lagrangian transport across the Gulf Stream (Bower 1991, Samelson 1992). In this model, the steady flow is described by the following stream function:

$$\Psi(x, y) = -\tanh \left\{ k \frac{y - B \cos(kx)}{\sqrt{1 + B^2 k^2 \sin^2(kx)}} \right\} + cy \quad (1)$$

where  $x$  and  $y$  are the fluid particle zonal and meridional coordinates, respectively,  $k$  is the wavenumber of the flow along the  $x$ -direction,  $B$  controls the amplitude of the meanders and  $c$  is the retrograde, counter stream, velocity component far from the jet's core which is centered on  $y = 0$ . The advective time,  $\tau_{adv}$ , is defined as the time needed for a particle, traveling close to the jet core, to move along the  $x$  direction a distance equal to the wavelength of the flow  $\lambda = 2\pi/k$ . For the typical values of the parameters used in our calculations, the value of this characteristic time is  $\tau_{adv} \simeq 4\pi$ . The recirculation time,  $\tau_{rec}$ , is defined as the period of a trajectory moving on a closed orbit next to the boundary of a gyre. This time is  $\tau_{rec} \sim 10 \cdot \tau_{adv}$ . The 2D incompressible velocity field  $(u, v)$  and the stream function  $\Psi(x, y)$

are related by,

$$u = -\frac{\partial\Psi}{\partial y}, \quad v = \frac{\partial\Psi}{\partial x}. \quad (2)$$

The flow is invariant under north-south inversion ( $y$  direction) and is periodic along the  $x$ -axis with period  $\lambda$ . In the absence of perturbations, passive particles follow the streamlines at constant  $\Psi$ . The steady flow corresponding to this stream function consists of open streamlines, to be identified as “the jet”, and closed streamlines, to be called “the gyres”, see Figure 1. Non-trivial behavior appears as soon as a perturbation is added to the above-described flow. In particular, cross-stream transport, i.e., from gyre to gyre, occurs either by the action of a random forcing or due to non-stochastic, time dependent terms inserted in the stream function which lead to the onset of Lagrangian chaos. In the stochastic model the position of a passive particle evolves according to

$$\frac{dx}{dt} = u(x, y) + w_1(t), \quad \frac{dy}{dt} = v(x, y) + w_2(t) \quad (3)$$

where the stochastic fields  $w_i(t)$  have red-noise correlations, i.e.,

$$\langle w_i(t)w_j(t') \rangle = 2\sigma^2\delta_{ij}e^{-|t-t'|/\tau}, \quad i, j = 1, 2, \quad (4)$$

with  $\sigma^2$  the variance of the stochastic fields and  $\tau$  their correlation time.

The deterministic, chaotic model is obtained by making the amplitude of the

meanders,  $B$  in equation (1), time dependent,

$$B \Rightarrow B(t) = B_0 + \epsilon \cos(\omega t + \phi) \quad (5)$$

where  $B_0$  is the mean meander amplitude and  $\epsilon$  and  $\omega$  are appropriately chosen so as to generate large-scale mixing, as in Cencini et al. (1999), i.e., leading to an overlap of resonances (Chirikov 1979);  $\phi$  is an arbitrary phase.

The symbolic dynamics (Beck and Schlögl 1993) of the noisy model can be satisfactorily approximated by a simple minded, first order Markov process. In the sequel we show that, in order to describe the chaotic dynamics via a first order Markov chain, it is necessary to introduce a more suitable definition of “state” which take into account the non trivial dynamical behavior of the system. This is made clear by comparing the symbolic dynamics generated by two different partitions of the phase space, both partitions having four cells.

The simple minded partition, call it  $\Pi$ , is defined by the southern gyre (symbol 1), the southern half jet (symbol 2), the northern half jet (symbol 3) and the northern gyre (symbol 4), see Figure 2. The partition takes into account the north-south symmetry as well as the periodicity of the system. The position of the advected particles is sampled millions of times at a time interval  $T = 2\pi/\omega$ . At each sampling time, one associates one of the symbols

according to the partition cell in which the particle is located at that time. In this way, a symbolic sequence is generated from each trajectory. Once this has been done, one computes the transition matrix  $W$ , giving the state-to-state transition probabilities in the time interval  $T$ .

While the precise nature of the perturbation, i.e., stochastic or purely deterministic, does not affect the gross qualitative features of the dispersion process, it does lead to very different correlation functions. In the deterministic, chaotic case, the transport process shows persistent, nontrivial long term correlations which are suppressed when stochastic noise is present. These differences are clearly seen in Figure 3. The  $W_{ij}$  matrix element is the probability to observe state  $j$  at time  $(n + 1)T$  knowing that the state  $i$  occurs at time  $nT$  (where  $n$  is integer). In the present case, using partition  $\Pi$ , this analysis leads to,

$$W = \begin{pmatrix} 0.851 & 0.147 & 0.002 & 0.000 \\ 0.247 & 0.535 & 0.215 & 0.003 \\ 0.003 & 0.215 & 0.535 & 0.247 \\ 0.000 & 0.002 & 0.147 & 0.851 \end{pmatrix}. \quad (6)$$

The symmetries in the transition matrix  $W$  reflect the dynamical and sta-

tistical equivalence of the northern and southern halves of the system. For future reference, we also quote the corresponding steady probability vector  $P = (P_1, P_2, P_3, P_4)$  which satisfies the equation

$$\sum_{i=1}^4 P_i W_{ij} = P_j \quad (7)$$

One finds: in the gyres,  $P_1 = P_4 = 0.315$ , and in the jet,  $P_2 = P_3 = 0.185$ .

In contraposition to the stochastic model defined by Eqs. (3) and (4), the deterministic evolution with (5) is characterized by long-term correlations which are poorly reproduced by the Markov chain generated from  $W$ . Essentially, the matrix elements  $W_{23}$  and  $W_{32}$  overestimate the coupling between the two halves of the systems. This failure of the simple probabilistic model based on  $W$  is illustrated in Figure 4 where the actual autocorrelation functions of the states 1 and 2 are compared with the corresponding correlation functions generated by the first order Markovian process described by  $W$ .

As one can see, in the actual dynamics there are basically two characteristic times,  $\tau_f$  and  $\tau_s$ , that correspond to the inverse of the two exponential decay rates at short and at long times, respectively. As order of magnitude, the shorter decay time is  $\tau_f \sim T$ , and the longer one is  $\tau_s \sim 10^2 \cdot T$ .

A way of estimating a lower bound for the order of the Markov chain which



would be necessary in order to adequately reproduce the system's statistical features, see, e.g., (Khinchin 1957), is based on the block entropies  $H_n$  which are defined by

$$H_n = - \sum_{C_n} P(C_n) \ln P(C_n),$$

where  $P(C_n)$  is the probability of observing a sequence  $C_n = (i_{t+1}, i_{t+2}, \dots, i_{t+n})$  of  $n$  successive symbols generated by the dynamical system, with  $i_m \in \{1, \dots, 4\}$  the partition cell visited at the time  $t = mT$ . From the block entropies  $H_n$  one computes next the quantities  $h_n = H_n - H_{n-1}$  which represent the average additional information needed to specify the  $n$ -th symbol  $i_n$  given the sequence  $C_{n-1}$ . The limit of  $h_n$  for  $n \rightarrow \infty$  gives the Shannon entropy  $h_S$  of the infinite sequence  $i_1, i_2, \dots$ . For a Markov process of order  $\nu$ , one has  $h_n = h_S$  for all  $n \geq \nu + 1$ , (Khinchin 1957). In agreement with what was found in the paper by Cencini et al. (1999), at least in order to reproduce the entropic properties, one would need a Markov process of very high order. Recall that this procedure gives only a lower bound to the order of the Markov chain. It is clear that the strategy consisting of simply increasing the order of the Markov process is not practical at all. Surprisingly, we were able to give a non-obvious choice of the partition that allows us to work with a first order Markov chain where now the time memory effects are

satisfactorily described. This is explained in the following. The new partition, denoted by  $\Pi^*$ , is a 4-state partition similar to the previous  $\Pi$  but the jet is partitioned in a different way: the jet corresponds to symbol 2 if the last previously visited cell is the southern gyre 1 or the cell 2 itself; if the last previously visited cell is the northern gyre 4 or the cell 3 itself, then the jet corresponds to symbol 3, see Figure 5. Accordingly, transitions between the two jet states 2 and 3 are not possible. This partition of the jet preserves part of the long time memory of the gyre-to-current transitions, a feature of the deterministic chaotic model which is impossible to reproduce with the previous partition  $\Pi$ . In other words, this partition introduces some memory even if formally the model remains of first order. The time signal generated by the  $\Pi^*$  Markov process is compared to the actual time signal in Figure 6. The memory effects are visible through the existence of “blocks” describing the fast back and forth gyre-to-current transitions in one half of the system, before moving to the other half. The new transition matrix  $W^*$  is found to

be,

$$W^* = \begin{pmatrix} 0.850 & 0.150 & 0.000 & 0.000 \\ 0.243 & 0.749 & 0.000 & 0.008 \\ 0.008 & 0.000 & 0.749 & 0.243 \\ 0.000 & 0.000 & 0.150 & 0.850 \end{pmatrix}. \quad (8)$$

The corresponding time-independent probability vector  $P^*$  is equal to the one found for the  $\Pi$  partition,  $P^* = P$ , as it should be. Notice that, because the transitions between states 1 and 2 (3 and 4) are much more frequent than those from state 3 to 1 (from 2 to 4), the matrix  $W^*$  is not far from being block-diagonal.

The improvements introduced by the  $\Pi^*$  partition show up in the correlation functions it generates, as can be seen in Figure 7, and in the fast convergence of the  $h_n$  entropies shown in Figure 8. Moreover, with the  $\Pi^*$  partition the two characteristic times are well estimated.

### 3 Conclusions

We have shown that the long-term memory effects which are present in the chaotic dispersion processes generated by the flow defined by Eqs. (1) and (5) can be reproduced by a Markov chain, provided that the partition of the

phase space is performed in a special way. It is important to remark that first order in a Markov process generated with the  $\Pi^*$  partition corresponds to a very large order, say  $\sim O(\tau_s/T)$ , in a Markov process generated from the  $\Pi$  partition. We hope that the ideas presented in this Note will be of use in a more general context and we plan to apply the above discussed technique to the analysis of other geophysical phenomena. Needless to say, when more than two characteristic times are relevant, partitions with a larger number of cells will be required.

## 4 Acknowledgements

R.A.P. acknowledges the hospitality of the Roman TNT group at University “La Sapienza”. A.V. acknowledges support from the INFM *Center for Statistical Mechanics and Complexity*.

## References

Beck, C. and F. Schlögl, 1993: Thermodynamics of chaotic systems. (*Cambridge University Press*, Cambridge UK).

Bower, A.S., 1991: A simple kinematic mechanism for mixing fluid parcels across a meandering jet. *J. Phys. Oceanogr.*, **21**, 173-180.

Cencini, M., G. Lacorata, A. Vulpiani and E. Zambianchi, 1999: Mixing in a meandering jet: a Markovian approximation. *J. Phys. Oceanogr.*, **29**, 2578-2594.

Chirikov, B.V., 1979: A universal instability of many-dimensional oscillator systems. *Phys. Rep.*, **52**, 263-379.

Crisanti, A., M. Falcioni, G. Paladin and A. Vulpiani, 1991: Lagrangian Chaos: Transport, Mixing and Diffusion in Fluids. *La Rivista del Nuovo Cimento*, **14**, 1-80.

Fraedrich, K., 1988: El Niño-Southern Oscillation predictability. *Mon. Wea. Rev.*, **116**, 1001-1012.

Khinchin, A.I., 1957: Mathematical foundations of Information Theory. *Dover*.

- Lorenz, E.N., 1963: Deterministic non-periodic flow. *J. Atmos. Sci.*, **20**, 130-141.
- Nicolis, C., W. Ebeling and C. Baraldi, 1997: Markov processes, dynamic entropies and statistical prediction of mesoscale weather regimes. *Tellus*, **49A**, 108-118.
- Ott, E., 1993: Chaos in dynamical systems. (*Cambridge University Press*, Cambridge UK).
- Ottino, J.M., 1989: The kinematics of mixing: stretching, chaos and transport. (*Cambridge University Press*, Cambridge UK).
- Samelson, R.M., 1992: Fluid exchange across a meandering jet. *J. Phys. Oceanogr.*, **22**, 431-440.
- Vautard, R., K. C. Mo, and M. Ghil, 1990: Statistical significance test for transition matrices of atmospheric Markov chains. *J. Atmos. Sci.*, **47**, 1926-1931.
- Yang, H., 1996: Chaotic transport and mixing by ocean gyre circulation. *Stochastic modelling in Physical Oceanography*, R.J. Adler, P. Muller and B.L. Rozovskii, Eds. Birkhäuser, 439-466.

## FIGURE CAPTIONS

FIGURE 1. Schematic diagram of the circulation in the meandering jet model. Arrows indicate the direction of particle motion: “westerly” advection in the jet current, clockwise and anti-clockwise recirculation in the southern and northern gyres, respectively. Spatial coordinates  $X$  and  $Y$  are given in unit of the wavelength  $\lambda = 2\pi/k$  and  $B_0$  is set equal to  $0.16\lambda$ , see eq. (1).

FIGURE 2.  $\Pi$  partition of the steady meandering jet: 1) south gyre; 2) south half-jet; 3) north half-jet; 4) north gyre.

FIGURE 3. Comparative plot of the two typical symbolic sequences obtained from: a) the stochastic model and b) the chaotic model, with the parameters in eq. (5) being  $\epsilon = B_0/4$  and  $\omega \simeq 2\pi/\tau_{adv}$ . The parameters of the red noise in eq. (4) are  $\sigma^2 = 6 \cdot 10^{-2}(\lambda/\tau_{adv})^2$  and  $\tau = T/4$ .

FIGURE 4. Autocorrelation functions for the states 1 and 2 of the  $\Pi$  partition, see Figure 2: actual autocorrelations from the chaotic model (full lines) and those generated by the transition-rate matrix  $W$  (dotted lines). Parameters of the deterministic perturbation: as in Figure 3.

FIGURE 5.  $\Pi^*$  partition of the steady meandering jet: 1) south gyre; 2) and 3) jet; 4) north gyre. The central jet corresponds to state 2 if the last visited

gyre is state 1, and to state 3 if the last visited gyre is state 4.

FIGURE 6 Comparative plot of: a) the chaotic model symbolic dynamics using the partition  $\Pi^*$  and b) the symbol sequence simulated on the basis of the transition-rate matrix  $W^*$ .

FIGURE 7. Autocorrelation functions for the states 1 and 2 of the  $\Pi^*$  partition, see Figure 5: actual autocorrelations from the chaotic model (full lines) and from the Markovian approximation generated with  $W^*$  (dotted lines).

FIGURE 8. Differential Block Entropy  $h_n = H_{n+1} - H_n$ , as a function of the sequence-length  $n$ , for the  $\Pi$  ( $\star$ ) and the  $\Pi^*$  ( $\square$ ) partitions. For each length  $n$  approximately  $\sim 10^7$  sequences were used. Notice the very different rate of convergence of  $h_n$  to its limit value (Shannon entropy)  $h_S$  in the two cases.



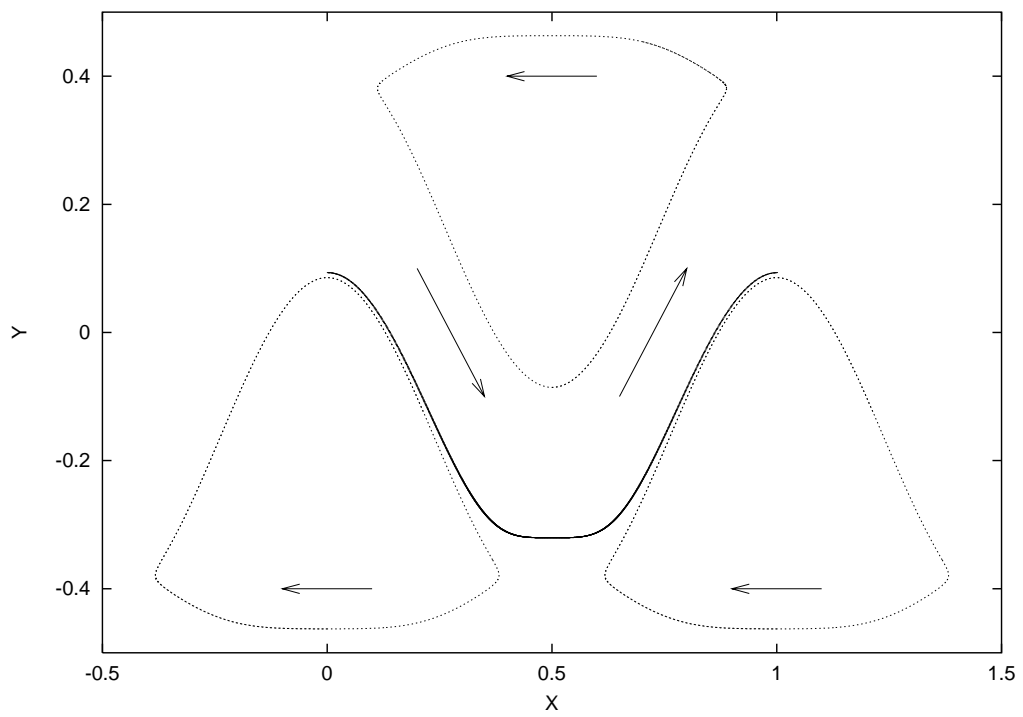


Figure 1:

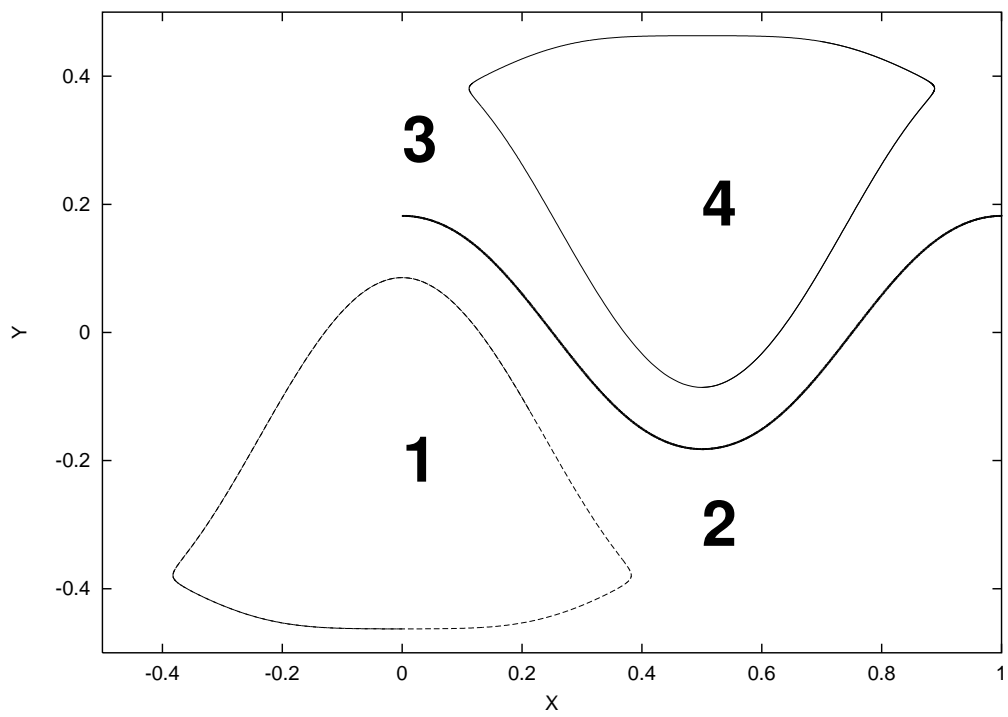
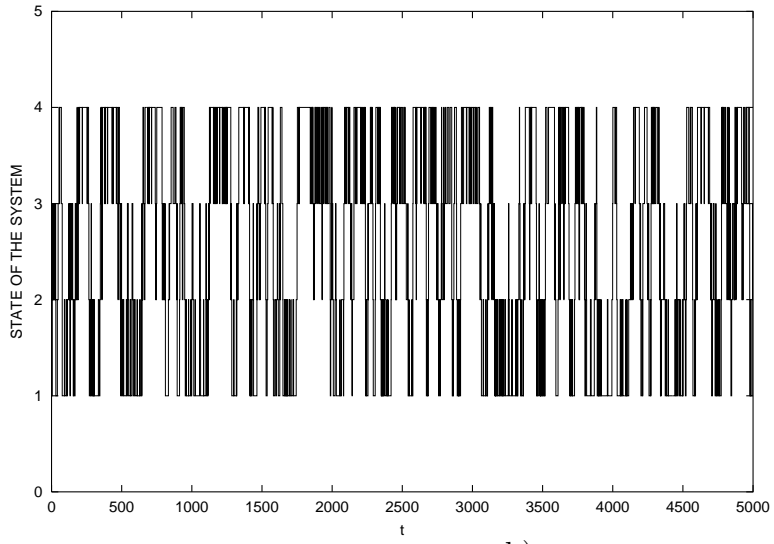


Figure 2:

a)



b)

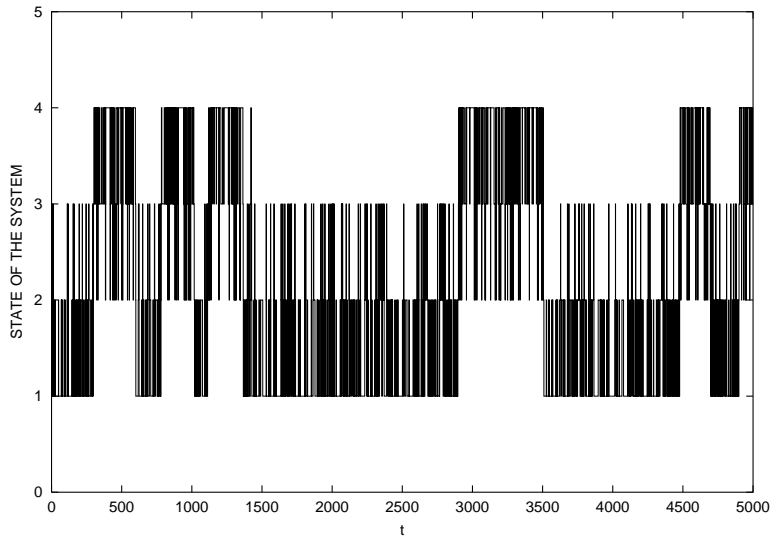


Figure 3:

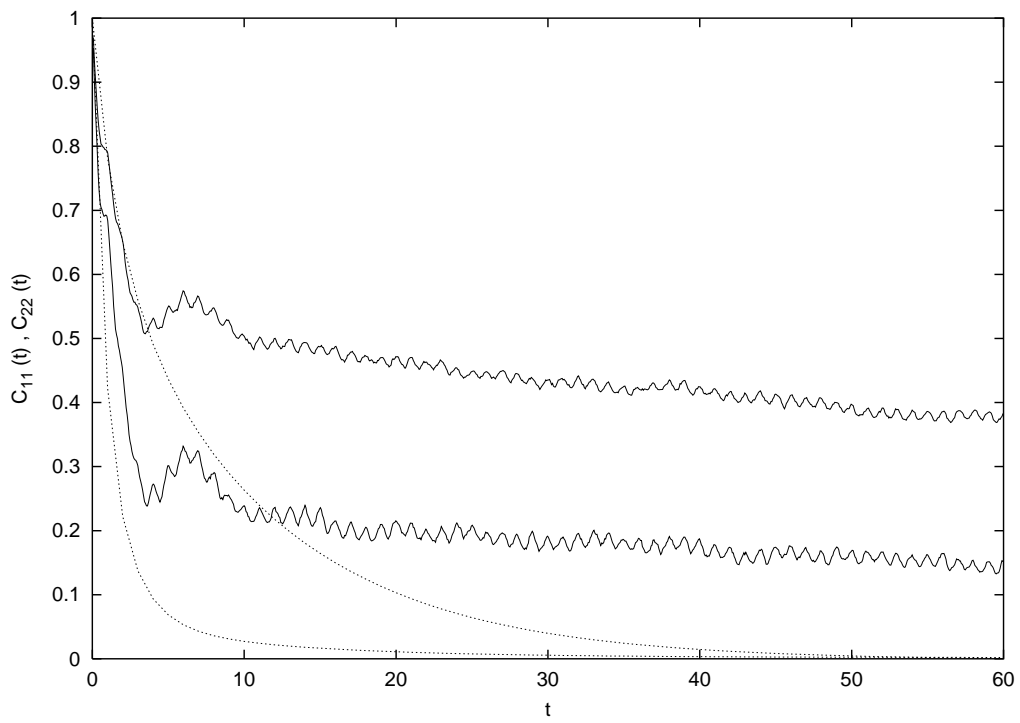


Figure 4:

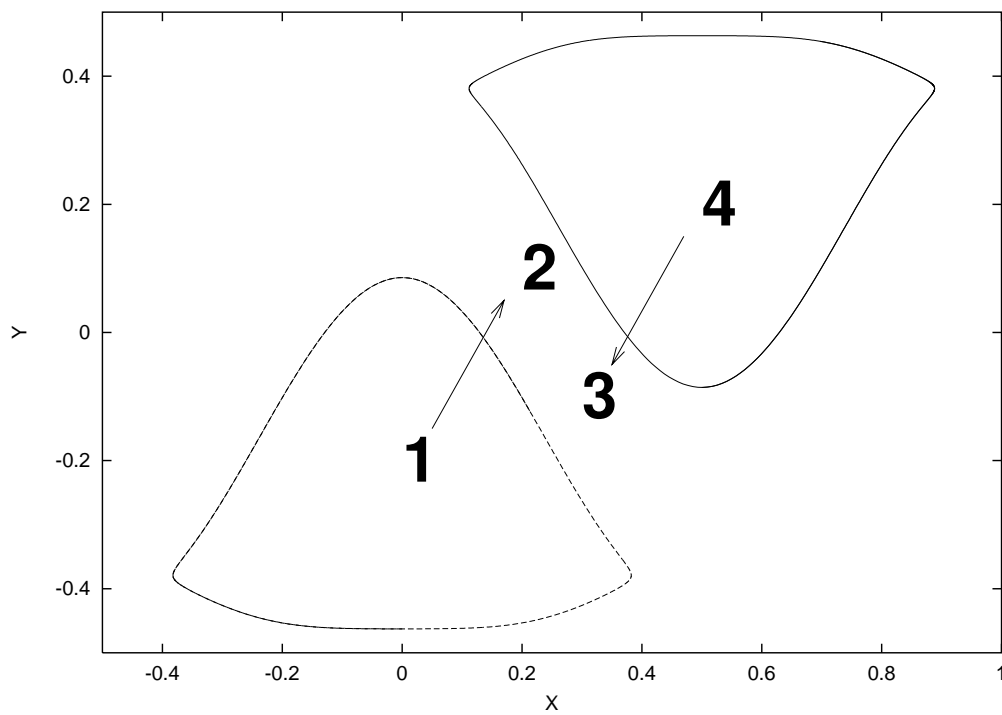
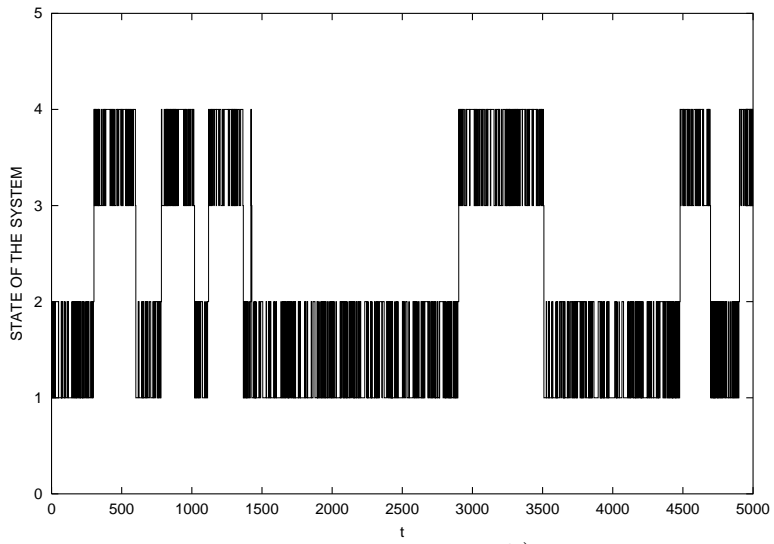


Figure 5:

a)



b)

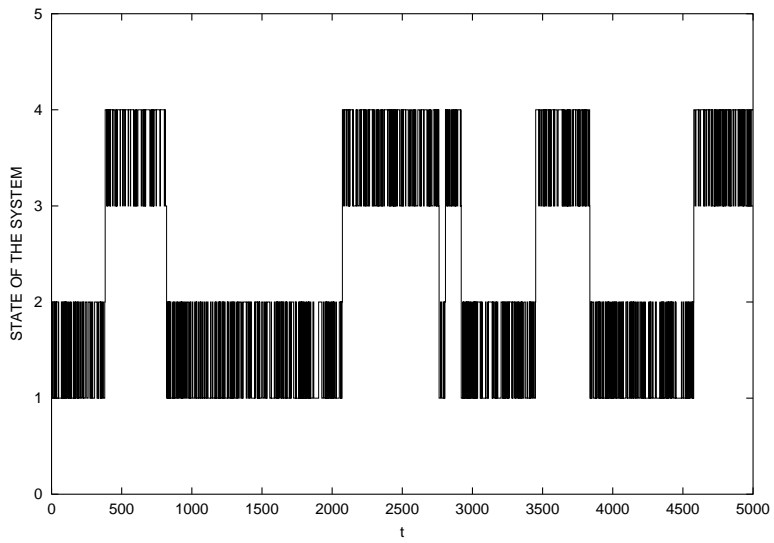


Figure 6:

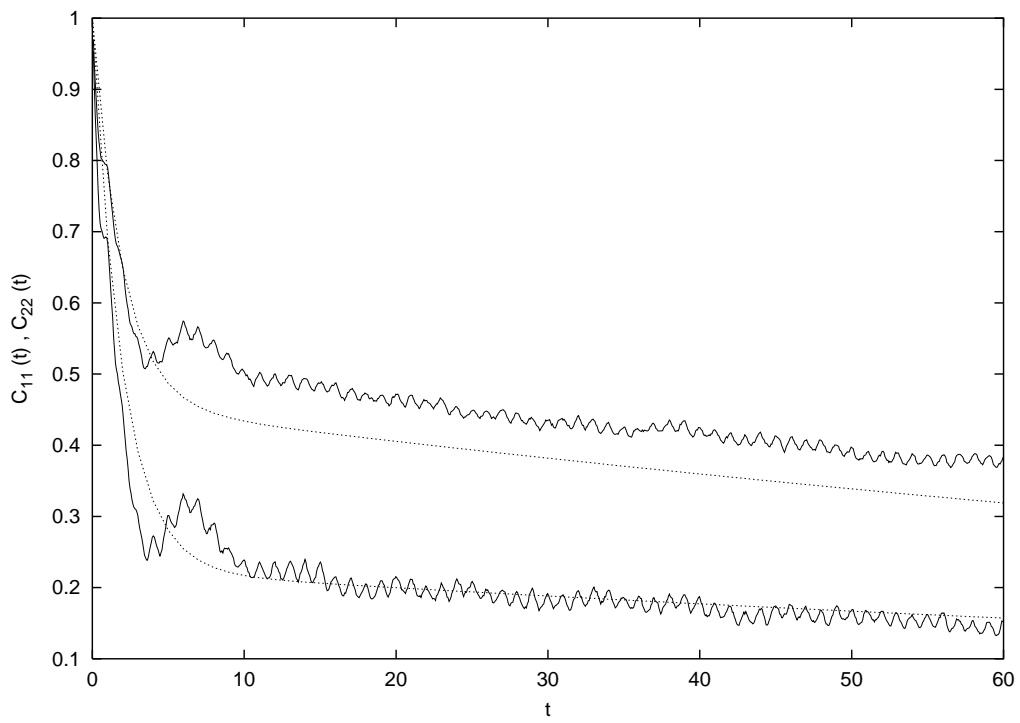


Figure 7:

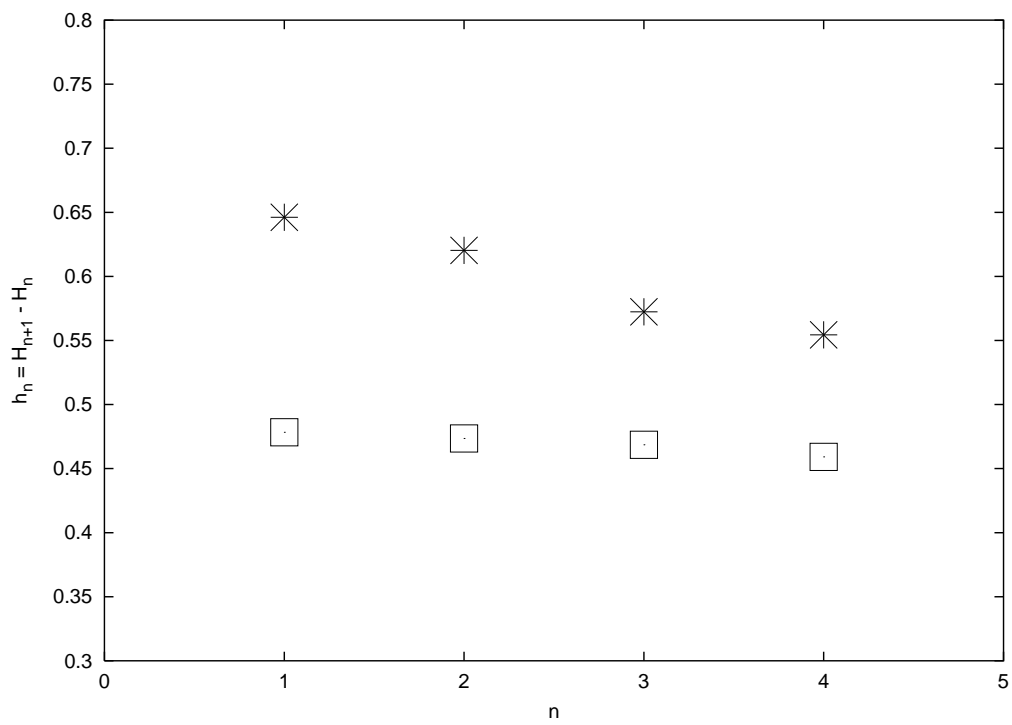


Figure 8: